Biorheology 44 (2007) 251–263
IOS Press

A fractional derivative model to describe arterial viscoelasticity

Damian Craiem * and Ricardo L. Armentano
Favaloro University, Facultad de Ingeniería, Ciencias Exactas y Naturales, Buenos Aires, Argentina

Received 20 April 2007
Accepted in revised form 7 August 2007

Abstract. Arterial viscoelasticity can be described with a complex modulus (E^*) in the frequency domain. In arteries, E^* presents a power-law response with a plateau for higher frequencies. Constitutive models based on a combination of purely elastic and viscous elements can be represented with integer order differential equations but show several limitations. Recently, fractional derivative models with fewer parameters have proven to be efficient in describing rheological tissues. A new element, called "spring-pot", that interpolates between springs and dashpots is incorporated. Starting with a Voigt model, we proposed two fractional alternative models with one and two spring-pots. The three models were tested in an anesthetized sheep in a control state and during smooth muscle activation. A least squares method was used to fit E^*. Local activation induced a vascular constriction with no pressure changes. The E^* results confirmed the steep increase from static to dynamic values and a plateau in the range 2–30 Hz, coherent with fractional model predictions. Activation increased E^*, affecting its real and imaginary parts separately. Only the model with two spring-pots correctly followed this behavior with the best performance in terms of least squares errors. In a context where activation separately modifies E^*, this alternative model should be considered in describing arterial viscoelasticity *in vivo*.

Keywords: Fractional calculus, complex modulus, constitutive models, arterial wall mechanics, viscoelasticity

1. Introduction

Arterial walls, as other soft biological tissues, are essentially viscoelastic. Main conduit arteries (i.e. aorta) have specific roles as hydraulic filters and cushioning pulsatile oscillations exerted by the ventricle. The structural composition of these arteries shows a functional predominance of elastic components. However, following a simultaneous pressure-diameter analysis, a hysteresis loop is evident, revealing a viscous behavior. The source of energy dissipation in the artery wall is associated primarily with smooth muscle cell content [9]. This energy dissipation (wall viscosity) is further increased with smooth muscle cell activation [2]. Smooth muscle activation can indeed continuously modify the wall structure by stretching elastic fibers within the artery wall.

Although several articles have described the viscoelastic properties of arteries *in-vitro*, few measurements have been made *in-vivo* [8,17,26,27,31]. Viscoelastic properties *in vivo* can be analyzed using a frequency dependent complex modulus. This complex modulus (E^*) has real and imaginary parts. The former is related to the elastic response of the material (i.e. storage modulus) and the latter (i.e. loss

*Address for correspondence: Dr. Damian Craiem, Universidad Favaloro, FICEN, Av. Belgrano 1723 (C1093AAS), Ciudad de Buenos Aires, Argentina. Fax: +54 11 43 84 07 82; E-mail: dcraiem@favaloro.edu.ar.

or dissipation modulus) to its viscous behavior. Storage and dissipation moduli in arteries show partial frequency independence within the physiologic range [9,11,18]. In contrast to pure elastic materials with complete frequency independence or pure viscous materials that exhibit an energy loss proportional to frequency, E^* in conduit arteries steeply increases from static values attaining a plateau at higher frequencies. Rheological lumped models are used to describe arterial mechanics in order to fit this frequency response. They are commonly based on a discrete arrangement of springs and dashpots (Kelvin–Voigt models). Even with generalized models, where the model order was increased to improve the fitting, some major limitations were reported [32].

Recently, classical viscoelastic models were generalized using fractional elements [4,22,28]. More importantly, constitutive equations of soft tissues and rheological models were extended using fractional order derivatives [12,14,21,30] and their theoretical basis was found to be mathematically consistent with molecular theories [5,6]. Based on the fractional calculus theory, a new type of element called *spring-pot* was incorporated into the constitutive equations. If in a pure elastic element, stress and strain are related by a zero order derivative (an elastic constant), and in a pure viscous dashpot by a first order derivative, a spring-pot renders the possibility of gradually interpolating between both by varying the order α of the element when $1 > \alpha > 0$. Moreover, in the frequency domain, a spring-pot behavior is intermediate between a constant elastic response and a viscous linear dependence, conforming to a weak power-law relationship over a wide range of frequency [23]. This response seems naturally predisposed for application to arterial mechanics problems. Furthermore, models based on fractional calculus have proven capable of describing more accurately complex structures [23,29] with fewer numbers of elements [30]. Finally, the new fractional element (spring-pot) could be easily integrated into classical Kelvin–Voigt constitutive equations so as to be associated with structural or physiological properties of the modeled soft tissue.

In the present work, we generalize a classical Voigt model using fractional calculus theory to describe the viscoelastic mechanical response of the aorta *in-vivo*. As far as we know, this methodology has not been applied before to characterize the mechanics of complete conduit arteries. A Voigt model (Model 1) was evaluated and compared to a modified version with one and two spring-pots (Models 2 and 3, respectively). Pressure and diameter measurements were invasively and continuously acquired with a previous validated methodology [1,3,7]. A topical application of phenylephrine was used to achieve vascular smooth muscle activation (isobaric analysis). The complex modulus (E^*) was calculated and fitted in the frequency domain. Components of Model 3 were stratified and the resulting values discussed.

2. Modeling

Assuming a linear theory, a complex modulus E^* can be derived to describe the viscoelastic properties of a material and its dependence on frequency (ω). Based on stress (σ) and strain (ε) measurements, E^* is defined as

$$E^*(\omega) = \frac{\sigma(\omega)}{\varepsilon(\omega)} = E_{\mathrm{S}}(\omega) + \mathrm{i}E_{\mathrm{D}}(\omega), \tag{1}$$

where $\mathrm{i}^2 = -1$ is the imaginary unit. The real part of $E^*(E_{\mathrm{S}})$ will be called storage modulus and the imaginary part (E_{D}) dissipation modulus. Storage and dissipation moduli in arteries are difficult to fit with classical spring-dashpot models because they show partial frequency independence over a wide frequency range.

The Voigt body is the simplest viscoelastic model that can store and dissipate energy, consisting of a perfectly elastic element (i.e. spring), arranged in parallel with a purely viscous element (i.e. dashpot). Its differential equation is:

$$\sigma(t) = E\varepsilon(t) + \eta\frac{\mathrm{d}\varepsilon(t)}{\mathrm{d}t},$$

where E denotes the elastic constant of the spring and η the viscous coefficient of the dashpot. Using Fourier transform and applying Eq. (1) we find E^* for this model:

$$E^*(\omega) = E + \mathrm{i}\eta\omega. \tag{2}$$

The limitations of this initial model are described elsewhere [24]. Briefly, this model shows creep but does not show relaxation, a behavior clearly observed in soft tissues. Moreover, the storage modulus would be constant and the loss modulus would increase proportionally to the frequency. In spite of these limitations, this simple model has been widely used because its two parameters are easily identified with the mechanical structure of a soft tissue. We will define the Voigt body as Model 1 (see Fig. 1).

Two alternative fractional derivative models will be proposed in this work. The most classical definition, attributed to Riemann and Liouville, for the fractional order ν derivative of a function $f(t)$ can be expressed as:

$$\frac{\mathrm{d}^\nu f}{\mathrm{d}t^\nu} = \frac{1}{\Gamma(1-\nu)}\frac{\mathrm{d}}{\mathrm{d}t}\int_0^t \frac{f(\tau)}{(t-\tau)^\nu}\,\mathrm{d}\tau, \tag{3}$$

where Γ is the Euler gamma function. Integer order derivatives are local operators. Following Eq. (3), the real order (fractional) derivative can be seen as the convolution of $\varepsilon(t)$ with a $t^{-\nu}$ function, anticipating

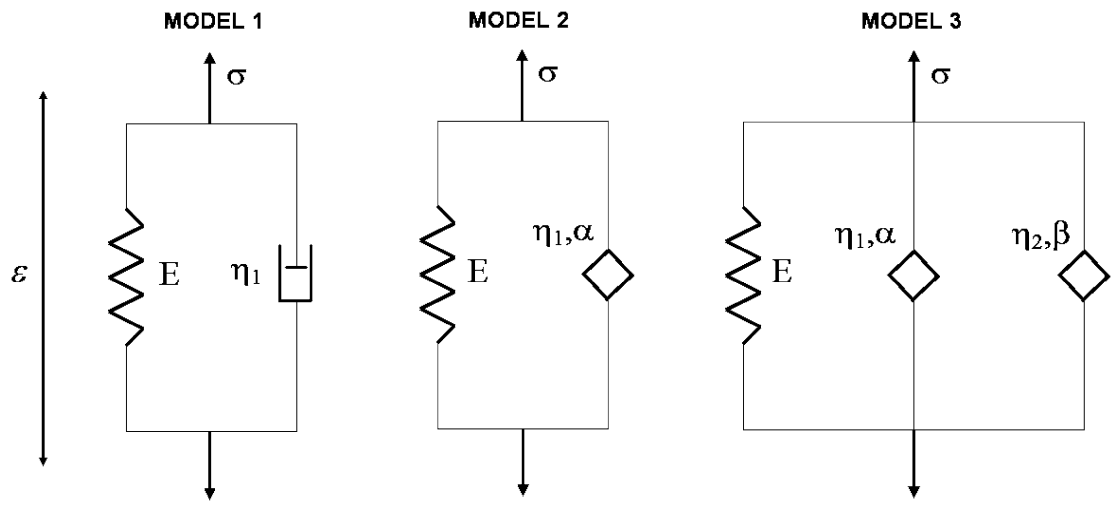

Fig. 1. Arrangement of springs, dashpots and spring-pots for the three proposed models. Model 1 = Voigt model. Model 2 = Fractional Voigt model with one spring-pot. Model 3 = Fractional Voigt model with two spring-pots.

some memory capability involved and power-law responses. Using this definition, a new element can be incorporated to the classical spring-dashpot pair called "spring-pot" [22] as follows:

$$\text{spring:} \quad \sigma = E\frac{\mathrm{d}^0\varepsilon}{\mathrm{d}t^0}, \qquad \text{dashpot:} \quad \sigma = \eta\frac{\mathrm{d}^1\varepsilon}{\mathrm{d}t^1}, \qquad \text{spring-pot:} \quad \sigma = \eta\frac{\mathrm{d}^\nu\varepsilon}{\mathrm{d}t^\nu}, \qquad 1 \geqslant \nu \geqslant 0,$$

where E and η are proportionality constants. The value of ν can be adjusted to interpolate between a pure elastic component ($\nu = 0$) and a pure viscous one ($\nu = 1$).

As a first alternative, we propose to replace the dashpot of Model 1 with a spring-pot (see Fig. 1). In this Model 2, the fractional derivative equation results:

$$\sigma(t) = E_0\varepsilon(t) + \eta_1\frac{\mathrm{d}^\alpha\varepsilon(t)}{\mathrm{d}t^\alpha}$$

and the complex modulus:

$$E^*(\omega) = \underbrace{\left[E_0 + \eta_1 \cdot \cos\left(\frac{\pi}{2}\alpha\right)\omega^\alpha\right]}_{storage} + \mathrm{i} \cdot \underbrace{\left[\eta_1 \cdot \sin\left(\frac{\pi}{2}\alpha\right)\omega^\alpha\right]}_{loss}. \tag{4}$$

Our last proposed Model 3 consists of a pure elastic spring and 2 spring-pots arranged in parallel (see Fig. 1), and can be presented in a constitutive fractional differential equation as:

$$\sigma(t) = E_0\varepsilon(t) + \eta_1\frac{\mathrm{d}\varepsilon^\alpha(t)}{\mathrm{d}t^\alpha} + \eta_2\frac{\mathrm{d}\varepsilon^\beta(t)}{\mathrm{d}t^\beta}. \tag{5}$$

Taking into account that the Fourier transform of a fractional derivative function $f(t)$ is $F[D^\nu f(t)] = (\mathrm{i}\omega)^\nu F[f(t)]$, Eq. (5) can be separated following Eq. (1) in its real and imaginary parts:

$$\begin{aligned} E^*(\omega) = {} & \underbrace{\left[E_0 + \eta_1 \cdot \cos\left(\frac{\pi}{2}\alpha\right)\omega^\alpha + \eta_2 \cdot \cos\left(\frac{\pi}{2}\beta\right)\omega^\beta\right]}_{storage} \\ & + \mathrm{i} \cdot \underbrace{\left[\eta_1 \cdot \sin\left(\frac{\pi}{2}\alpha\right)\omega^\alpha + \eta_2 \cdot \sin\left(\frac{\pi}{2}\beta\right)\omega^\beta\right]}_{loss}. \end{aligned} \tag{6}$$

The influence of each term in Eq. (6) will be analyzed during smooth muscle activation separately to study the role of each element in this fractional model.

3. Experimental evaluation

3.1. Instrumentation

All protocols were approved by the Research and Development Council of the Favaloro University (Argentina) and were conducted in accordance with the National Institutes of Health Guidelines for the

care and use of laboratory animals (NIH Publication No. 85-23, revised 1996). The surgical procedure has been previously described in detail [7]. A Merino sheep, weighing 60 kg was selected for this study. Anesthesia was induced with intravenous thiopental sodium (20 mg/kg), and was maintained with 2.5% enflurane carried in pure oxygen (4 l/min) through a Bain tube connected to a respirator. Both pressure (model P3.5, 1200 Hz frequency response, Konigsberg Instruments, Inc., Pasadena, CA) and diameter (ultrasonic crystals, 5 MHz, 3 mm diameter) sensors were implanted in the same ring of a descending thoracic aorta. Signals were digitized at a frequency rate of 250 Hz (12 bits) for off-line processing. Vascular muscle activation was induced using phenylephrine (PHE) (0.5 ml) dosed locally over the aortic segment. The activation measurements during PHE were made after the vascular constriction was stabilized. Measurements were made with the respirator turned off during 10 seconds for both CTL and PHE.

3.2. Stress–strain derivation

Aortic strain (ε) and stress (σ) were calculated from the measured pressure (P) and external radius (r_{e}) as previously reported [7]. Briefly, assuming a thick walled cylindrical geometry, the following equations can be defined,

$$\varepsilon = \frac{R}{R_0},$$

$$\sigma = 133.4 \frac{2P(r_{\mathrm{e}} r_{\mathrm{i}})^2}{r_{\mathrm{e}}^2 - r_{\mathrm{i}}^2} \frac{1}{R^2},$$

where R is the midwall radius calculated as $R = (r_{\mathrm{e}} + r_{\mathrm{i}})/2$, R_0 is the unstressed mid-wall radius measured right after the sacrifice during autopsy (approximately at 25 mmHg of aortic remaining pressure), 133.4 is a conversion constant to report the stress in Pa and r_{i} is the internal radius calculated as:

$$r_{\mathrm{i}} = r_{\mathrm{e}}^2 - \frac{V}{\pi L},$$

where V is the volume of the segment of length L. This length was measured during surgery between two adjacent marks sutured to the aortic segment using a caliper. This segment was then carefully dissected free from surrounding tissue, cut at the markers, and weighed on a precision balance. V was calculated using the weight of the aortic wall segment and assuming a tissue density of 1.066 g/ml [13].

Periods of both pressure and diameter signals were automatically separated and converted to stress strain. Fifty representative cycles were selected in CTL and during activation with PHE. Fourier transform was applied to an averaged period to obtain measurements of the real and imaginary parts of E^* in Eq. (1). Heart rate was near 2 Hz. A frequency range of 30 Hz was adopted, including the first 15 significant harmonics. To obtain the parameters of Model 1 in Eq. (2), storage modulus points were averaged to obtain E and dissipation modulus values were interpolated to a linear function to obtain the η (slope). For fractional models 2 and 3, Eqs (4) and (6) were fitted to the real and imaginary parts of E^* simultaneously using the trust region method for nonlinear least squares minimization, based on the interior-reflective Newton method (lsqcurvefit function from Matlab©). Parameters were compared for CTL and during activation with PHE.

The complex modulus was then normalized to E_0 such that $E(\omega = 0) = 1$. Additionally, least squares error (*LSE*) defined as

$$LSE[\%] = \sqrt{\left(\sum_{i=0}^{15}[E^*_{\text{measured}}(\omega_i) - E^*_{\text{model}}(\omega_i)]^2\right) \Big/ \left(\sum_{i=1}^{15} E^*_{\text{measured}}(\omega_i)^2\right)} \times 100 \tag{7}$$

was calculated over the first 15 normalized harmonics to evaluate the spectrum fit for the real and imaginary parts.

To further evaluate the viscoelastic model fit, a vector diagram that is traditionally used in mechanical engineering was constructed using the 15 real and 15 imaginary points of the normalized E^* results. This diagram was constructed for Model 3 by combining the harmonics of the storage modulus in the abscissa and the harmonics of the loss modulus in the ordinate. This curve facilitates the identification and classification of materials, and helps to visualize in the same graphic the relation between the real and imaginary parts of E^* and the frequency [28].

3.3. Model fitting

Pressure-diameter and stress-strain loops are shown in Fig. 2 for both CTL and PHE. The topical application of PHE locally activated the smooth muscle, contracting the artery without changes in pressure (left). Stress and strain diminished concomitantly (right). The resulting hysteresis confirm the natural viscous behavior of the aortic wall.

Table 1 shows the parameter fit in each viscoelastic model. During PHE, the static elastic modulus E_0 and the proportionality viscous factors (η_1 and η_2) increased in all cases, whereas in Model 2 and Model 3 the order α diminished, in Model 3 β remained stable. The values of E^* at high frequencies averaged 520 kPa for CTL and 640 kPa during PHE, whereas the phase response attained a plateau of 12 and 17 degrees respectively. Real and imaginary parts of the E^* for all models are presented in Fig. 3 as ratio normalized moduli (E^*/E_0). Potential curves can be confirmed in storage moduli with significant

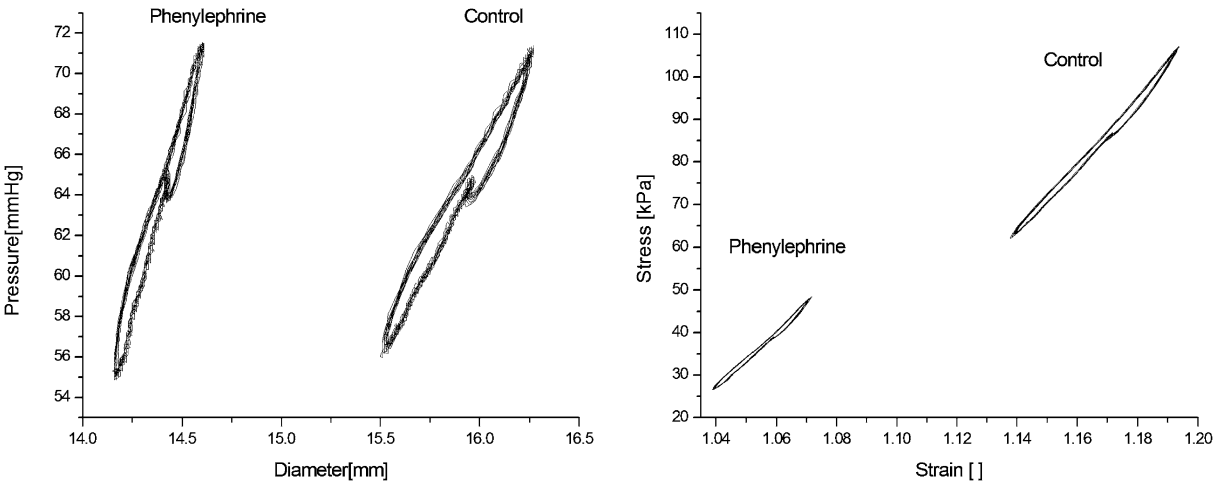

Fig. 2. Pressure-diameter (left) and stress-strain (right) *in-vivo* loops for the anesthetized sheep in control (CTL) and during smooth vascular activation with phenylephrine (PHE).

Table 1

Viscoelastic results after least squares fit of the real and imaginary parts of the complex modulus E^* in the frequency domain (15 harmonics). Model 1 = Voigt model. Model 2 = Fractional Voigt model with one spring-pot. Model 3 = Fractional Voigt model with two spring-pots. CTL, Control state. PHE, Local smooth muscle activation with phenylephrine. r^2 = Pearson correlation coefficient

		E_0 (kPa)	α	η_1 (kPa s$^\alpha$)	β	η_2 (kPa s$^\beta$)	r^2, p
MODEL 1	CTL	481	1	0.7			0.47, $p < 0.05$
	PHE	573	1	1.2			0.62, $p < 0.05$
MODEL 2	CTL	393	0.51	12.1			0.82, $p < 0.01$
	PHE	411	0.42	39.8			0.95, $p < 0.01$
MODEL 3	CTL	393	0.20	32.6	0.84	1.07	0.77, $p < 0.01$
	PHE	411	0.11	82.2	0.80	2.73	0.93, $p < 0.01$

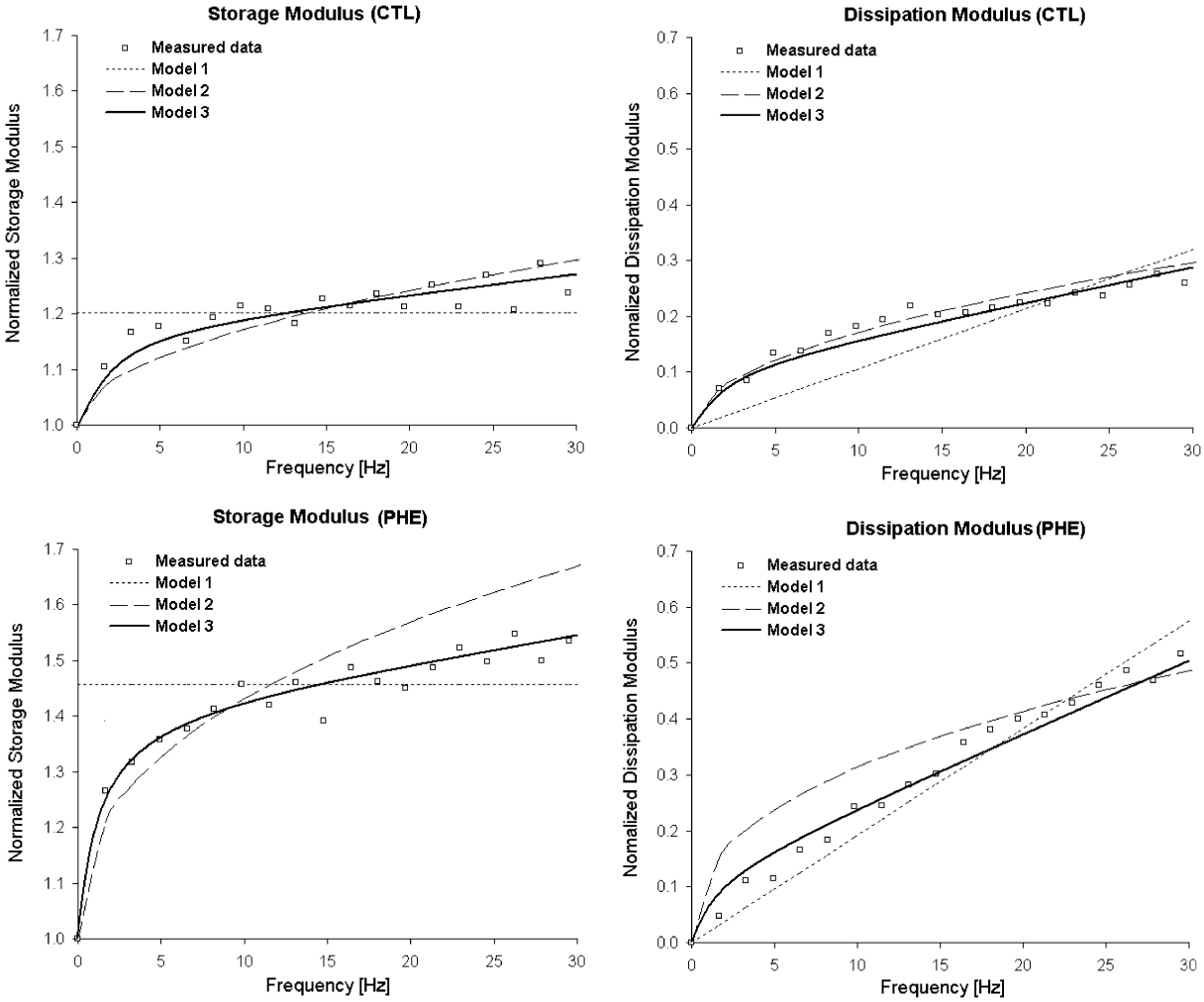

Fig. 3. Real (storage modulus) and imaginary (dissipation modulus) parts of the complex modulus (E^*) in control (CTL) and during smooth vascular activation with phenylephrine (PHE). Data (empty squares) and model results (lines) after least square fit.

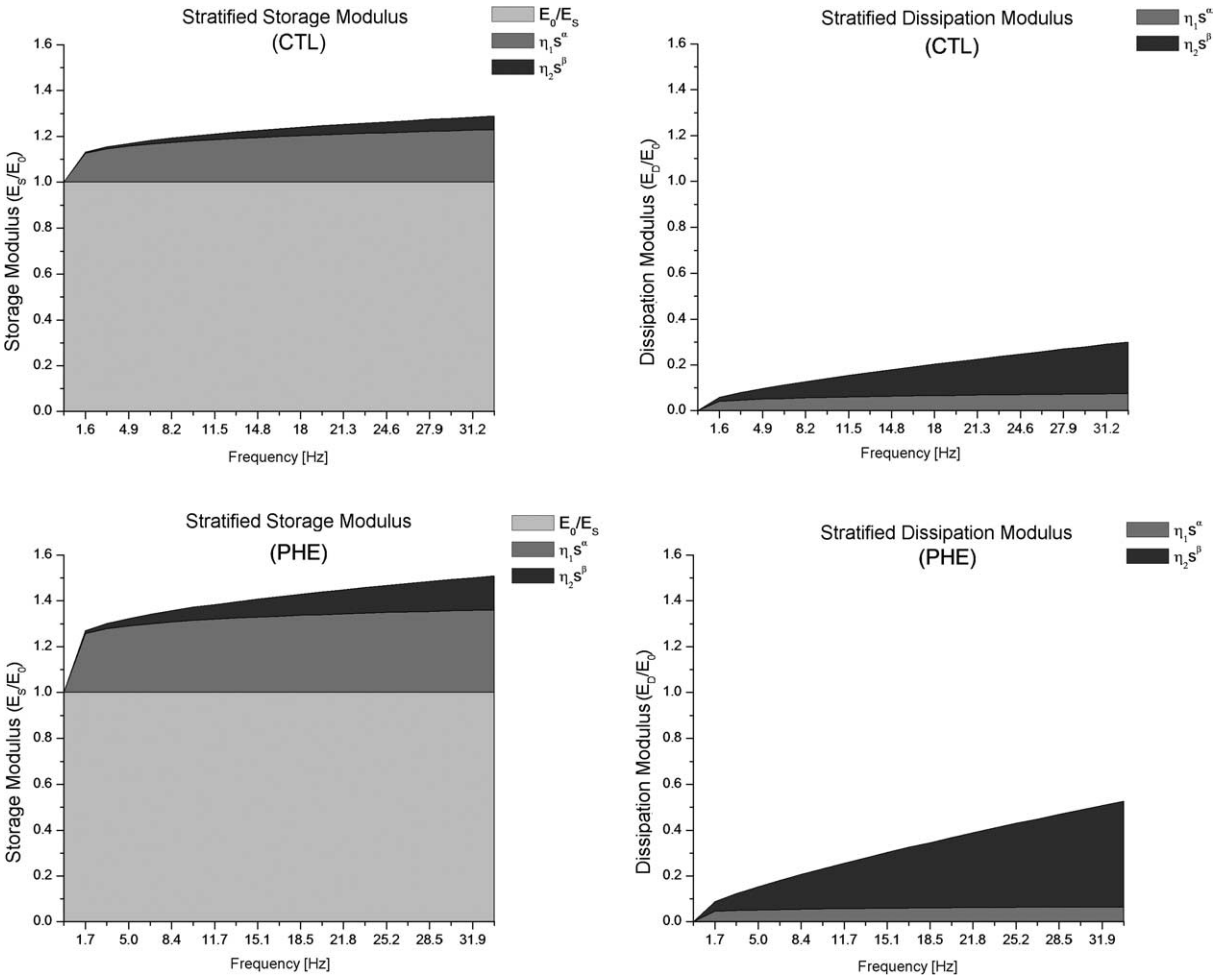

Fig. 4. Stratified storage and dissipation moduli, from real and imaginary parts of the complex modulus of the fractional Model 3 in Eq. (6) during control (CTL) and smooth muscle activation (PHE).

increments during PHE with respect to CTL. Dissipation modulus during PHE showed a more linear frequency dependence with respect to CTL behavior, where a power-law function was clearly visible.

For Model 3, the magnitudes of each term from Eq. (6) are shown in Fig. 4. The importance of the elastic spring is evident in both storage moduli. In this model, an elastic predominance can be seen for the $\eta_1 - \alpha$ spring-pot in contrast to the more dissipative $\eta_2 - \beta$ fractional element. The major contribution of the latter in the dissipation modulus during PHE could be seen. Finally, a vector diagram was constructed from the real and imaginary parts of E^* in Model 3 and is presented in Fig. 5 for measured data and calculated model results. The harmonics values were connected with lines. Measured and modeled values are reasonably congruent although measured values have increasing dispersion at higher frequencies. As defined by Eq. (7), LSE for storage and dissipation moduli during CTL were Model 1: 27% and 15%, Model 2: 5% and 9%, Model 3: 3% and 8%, and during PHE were Model 1: 48% and 77%, Model 2: 8% and 19%, Model 3: 2% and 9%, respectively.

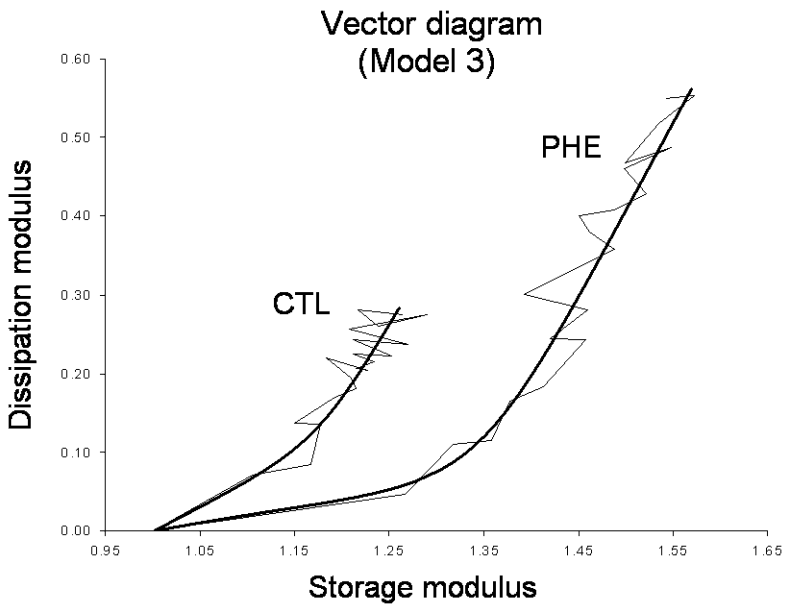

Fig. 5. Vector diagram composed by the storage modulus in the abscissa axis and the dissipation modulus in the ordinate axis. Comparison of experimental data (thin line) and the fractional Model 3 with 2 spring-pots (thick line) for control (CTL) smooth vascular activation (PHE).

4. Discussion

This work shows that fractional derivative models adequately describe the mechanical response of the arterial wall *in-vivo* both during control and smooth muscle activation states. The best empirical agreement between the measured and modeled E^* for Model 3 suggests that the incorporation of two spring-pots to the classical Kelvin–Voigt scheme should be considered and discussed as an alternative to model arterial viscoelasticity.

To analyze the arterial wall mechanics, a complex modulus (E^*) approach was adopted. Linear viscoelasticity assumes that stress is a function of strain history. In the frequency domain, this hypothesis is equivalent to the existence of a complex modulus such that $\sigma(\omega) = \varepsilon(\omega)E^*(\omega)$. From a practical point of view, viscoelasticity problems can be solved by fitting a model to the frequency dependent E^*. In many soft tissues, and particularly in arteries, E^* increases rapidly with frequency attaining a plateau, when it becomes almost frequency independent [9,11,24]. The storage modulus for high frequencies during CTL (5×10^6 dyn $\cdot$ cm^{-2}) resulted somewhat higher compared to other reports in adult sheep: 3×10^6 dyn $\cdot$ cm^{-2} [17], 3.5×10^6 dyn $\cdot$ cm^{-2} [25], 3.3×10^6 dyn $\cdot$ cm^{-2} [31] but more compatible with previous reports from our group [16]: 4.4×10^6 dyn $\cdot$ cm^{-2}. Differences may be principally due to animal specimens, particular methodologies, anesthesia and the arterial segment considered.

As remarked by Bergel [9] many attempts were made to fit E^* to simple models, linearly combining ideal springs and dashpots. The simplest Voigt option was adopted in Model 1. Following Eq. (2), the storage modulus is described with a constant value and the dissipation modulus linearly increases with frequency. As seen in Fig. 3, this model is poorly adapted to measured data. The quality of fit can be improved increasing the number of elements although this tendency systematically blurs the physical meaning of the increased number of parameters [32]. In fact, previous reports from our group used adaptive models to fit E^* but the number of parameters was reduced to ensure a proper analysis [16].

Others studied structural damping, also called hysteretic damping, considering a complex stiffness that is completely frequency independent [19]. This formulation is based on the Hilbert transform, but as arteries are not completely frequency independent they cannot be applied directly.

Lumped models constructed with fractional derivative elements appear as an alternative [23]. They were shown to be an intimate descriptor of rheological materials with few parameters. As described in the modeling section, elements that interpolate between ideal springs and dashpots can be conceived using fractional order derivatives. They are called spring-pots. Their fractional order can be adjusted between integer orders 0 (spring) and 1 (dashpot).

In Model 2, a dashpot (order 1) was replaced with a spring-pot (order α). The order α for CTL and PHE resulted $\sim$0.45, confirming an intermediate behavior. In spite of the important improvement observed during CTL in both storage and dissipation moduli, the frequency dependence during acute smooth muscle activation could not be properly adapted as seen in Fig. 3. The main reason might be analyzed observing the imaginary part of E^*. While the storage modulus proportionally increased during activation with respect to CTL, the dissipation modulus described a more pronounced linear frequency dependence. This particular behavior is not contemplated in Eq. (4), where both real and imaginary parts of E^* depend on a unique ω^α power-law function. In spite of this limitation, LSE results confirmed an important reduction with respect to Model 1.

Model 3, with an ideal spring and 2 spring-pots, showed the best agreement with measured data. These results can be confirmed in Fig. 3 and evaluating LSE results that never exceeded 9%. More importantly, the model was not arbitrarily chosen. It was designed to adapt its parameters to physiological conditions (CTL) and during smooth muscle activation (PHE). It appears as an extension of the rheological cell model introduced by Fabry [15] and further explained by fractional derivative viscoelasticity [12]. In previous works of our group, a modified Voigt model was proposed to model the arterial wall *in-vivo* [1]. Following our experience, the incorporation of two fractional elements with adjustable orders, allowed us to better describe the arterial wall behavior in both control and active states giving some physiological meaning to each parameter.

Why two spring-pots? Storage and dissipation moduli (see Fig. 3) followed a different behavior during smooth muscle activation (PHE). That is why 2 fractional elements were proposed in our model. Storage modulus increased with increasing frequency according to a weak power-law (order 0.2) during CTL and increased in a proportion to the frequency during PHE. Loss modulus also followed a power-law response during CTL but with a more pronounced frequency dependence during PHE. Observing Eq. (6), a partial independence between real and imaginary parts was allowed incorporating a second spring-pot, with respect to Eq. (4) (Model 2).

At this moment, we can interpret the parameters of Model 3. The structural elasticity of the wall, independent of muscle activation, was represented with the ideal spring E_0. The first spring-pot, characterized by η_1, α parameters, became predominantly elastic ($\alpha \approx 0.2$) and might be associated with the elastic contribution of vascular smooth muscle. As can be deduced from Eq. (6), for orders of α closer to zero, the cosine function ensures a significant influence of this spring-pot on the storage response, whereas the sine function forecasts a negligible participation on loss modulus. At this point, our results do not differ from others who used fractional models to describe biological soft tissues. In airway cultured smooth muscle cells [12], lung [30] and canine liver tissues [21] the fractional order was about 0.1–0.2, close to the values of our η_1, α spring-pot parameters. The second spring-pot, described by η_2, β parameters, can be associated with a dissipating element, where a clear viscous behavior was found ($\beta \approx 0.8$). In this case, a corresponding influence in the dissipation modulus was expected, associated with the sine function influence for $\beta \approx 0.8$ in Eq. (6). Viscosity is partly responsible for the frequency

dependence of E^*. Particularly in arteries, different sources of viscosity can be predicted, including the intrinsic cellular contribution and vascular smooth muscular action. Also, the myogenic response can contribute *in-vivo*.

Phenylephrine was used to locally activate the smooth muscle of the arterial segment without disturbing pressure values, whereas there was a strong vasoconstriction (Fig. 2). Vascular smooth muscle can modulate this elastic-viscous contribution in conduit arteries [1]. The physiological relevance of this energy dissipation in conduit arteries is still controversial [10]. Although the magnitude of the viscous energy involved in this process seems to be negligible, its integration along the arterial tree can indeed enhance its influence [32]. Even if the aorta does not likely undergo this kind of powerful local vasoconstriction *in-vivo* as seen in Fig. 2, smooth muscle activation experiments here were helpful in assessing their role in wall viscoelasticity.

Smooth muscle activation produced simultaneous effects of increasing storage and loss moduli, and in the latter a stronger frequency dependence was evident. These effects were reflected in the first spring-pot with a reduction of α and an increment in η_1, making it more elastic with barely any viscous contribution. In the second spring-pot, where the fractional order remained near $\beta \approx 0.8$ during PHE, a three-fold increase in η_2 was evident.

To get further insight into the particular role of each element of the model, E^* in Eq. (6) was decomposed into 5 terms and their magnitudes were shown in Fig. 4. Analyzing the storage modulus (real part of Eq. (6) and left side of Fig. 4), the predominant elastic contribution depended on the pure elastic spring E_0 and the most elastic spring-pot (η_1, α). This spring-pot can represent the smooth muscle elastic participation in the arterial response *in-vivo*. Activation reduced the fractional order (more elastic) and increased the proportional factor (η_1). On the other hand, dissipation moduli were prone to depend on the most viscous spring-pot (η_2, β). Activation did not change the second spring-pot order β that remained stable near pure viscous values, but significantly increased its proportionality factor η_2, confirming an energy dissipation effect. These results suggest that the first spring-pot might describe the interrelation between the contractile muscle cells stretching the elastic fibers and modulating their elastic contribution. The second spring-pot seems to represent a more pure structural viscous behavior, with no order change during activation, but with a significant participation in arterial energy dissipation. These initial hypotheses conform with the idea of a serial elastic component (SEC) defined as the algebraic sum of all coupled muscle components in the force generating apparatus and the existence of a contractile element [1,13].

The ability of Model 3 to fit simultaneously the storage and loss moduli was also verified using a vector diagram (Fig. 5). Vector diagrams are traditionally used in mechanical engineering. They simultaneously show the relation between the real and imaginary parts of E^*. Our vector diagram correctly matches the modified Kelvin–Voigt model (with 2 fractional operators) described in a complete review of fractional models of two (or more) elements made by Rossikhin and Shitkova [28]. This is consistent with normalized storage and loss moduli responses. The former starts, for static values, at 1 and the latter at zero, whereas both increase with frequency to attain a similar plateau approximately 30% higher in CTL and 60% during PHE (Fig. 3). That explains why the vector diagram describes an open curve that starts at $(1, 0)$ and finishes at $(1.3, 0.3)$ for CTL and at $(1.6, 0.3)$ for PHE. The particular concave contour of the vector curve confirms that the storage modulus increases more rapidly with frequency than the loss modulus. The latter has a more linear frequency dependence that might be associated with the underlying dissipation process.

In contrast to *in-vitro* studies, our *in-vivo* experiments yielded information from the mechanical properties of the living animal where the complete artery remained intact with all the natural variability.

Although this methodology is attractive to describe physiological events, some limitations must be emphasized. E^* in the living animal was determined at a mean distending pressure for multiples of the heart rate and variations around this working point were considered. While non-linear behavior of the arterial wall is well reported, strains were considered small under stable physiologic conditions, supporting the assumption of a linear approximation. The arterial wall constituents are essentially elastin, collagen and smooth muscle. We assumed that at low pressure values, as those found in the anesthetized sheep (Fig. 2), the mechanical response was mainly governed by the elastic behavior. Consequently, a linear model was adopted permitting the complex modulus analysis to be a reasonable approach. The absolute and normalized values for the E^* *in-vivo* did not differ from others [24,27,31,32] and resulted in findings comparable to those *in-vitro* [11].

Finally, although no stress relaxation experiments are allowed *in-vivo*, the proposed fractional model could be used to predict it. Just as the exponential function appears as the solution to integer order differential equation, potential functions of the form $t^{-\alpha}$ can be obtained by solving Eq. (5) for a step in strain. These power-law responses offered by the fractional order model, with a pronounced descent and a very slow relaxation, seem to be more appropriate to model stress-relaxation results in arteries than the classical exponential result from integer order equations [20,23]. Future stress-relaxation experiments will be needed to test fractional models *in-vitro* so as to complement our findings *in-vivo*.

Acknowledgements

We would like to thank Dr. Juan G. Barra who was in charge of the surgery. This work was partly supported by a doctoral fellowship from the National Technologic University in Argentina (UTN-Rectorado) and by BID 1201/OC-AR/PICT # 14334 of the Secretaría de Ciencia, Tecnología e Innovación Productiva (Argentina).

Help and useful comments from Dr. Patrice Flaud (ECOS-Sud Argentina/France No.: A06S02) are also acknowledged.

References

[1] R.L. Armentano, J.G. Barra, J. Levenson, A. Simon and R.H. Pichel, Arterial wall mechanics in conscious dogs. Assessment of viscous, inertial, and elastic moduli to characterize aortic wall behavior, *Circ. Res.* **76** (1995), 468–678.

[2] R.L. Armentano, J.G. Barra, D.B. Santana, F.M. Pessana, S. Graf, D. Craiem, L.M. Brandani, H.P. Baglivo and R.A. Sanchez, Smart damping modulation of carotid wall energetics in human hypertension: effects of angiotensin-converting enzyme inhibition, *Hypertension* **47** (2006), 384–390.

[3] R.L. Armentano, J. Levenson, J.G. Barra, E.I. Fischer, G.J. Breitbart, R.H. Pichel and A. Simon, Assessment of elastin and collagen contribution to aortic elasticity in conscious dogs, *Am. J. Physiol.* **260** (1991), 1870–1877.

[4] T.M. Atanackovic and B.N. Novakovic, On a fractional derivative type of a viscoelastic body, *Theor. Appl. Mech.* **28** (2002), 27–37.

[5] R.L. Bagley and P.J. Torvik, A theoretical basis for the application of fractional calculus to viscoelasticity, *J. Rheol.* **27** (1983), 201–210.

[6] R.L. Bagley and P.J. Torvik, On the fractional calculus model of viscoelastic behavior, *J. Rheol.* **30** (1986), 133–155.

[7] J.G. Barra, R.L. Armentano, J. Levenson, E.I. Fischer, R.H. Pichel and A. Simon, Assessment of smooth muscle contribution to descending thoracic aortic elastic mechanics in conscious dogs, *Circ. Res.* **73** (1993), 1040–1050.

[8] R.D. Bauer, Rheological approaches of arteries, *Biorheology*, Suppl. 1 (1984), 159–167.

[9] D.H. Bergel, The dynamic elastic properties of the arterial wall, *J. Physiol.* **156** (1961), 458–469.

[10] D. Bia, R.L. Armentano, D. Craiem, J. Grignola, F. Gines, A. Simon and J. Levenson, Smooth muscle role on pulmonary arterial function during acute pulmonary hypertension in sheep, *Acta Physiol. Scand.* **181** (2004), 359–366.

[11] R.H. Cox, Viscoelastic properties of canine pulmonary arteries, *Am. J. Physiol.* **246** (1984), 90–96.

[12] V.D. Djordjevic, J. Jaric, B. Fabry, J.J. Fredberg and D. Stamenovic, Fractional derivatives embody essential features of cell rheological behavior, *Ann. Biomed. Eng.* **31** (2003), 692–699.
[13] P.B. Dobrin and A.A. Rovick, Influence of vascular smooth muscle on contractile mechanisms and elasticity of arteries, *Am. J. Physiol. Heart Circ. Physiol.* **217** (1969), 1644–1651.
[14] T.C. Doehring, E.O. Carew and I. Vesely, The effect of strain rate on the viscoelastic response of aortic valve tissue: a direct-fit approach, *Ann. Biomed. Eng.* **32** (2004), 223–232.
[15] B. Fabry, G.N. Maksym, J.P. Butler, M. Glogauer, D. Navajas and J.J. Fredberg, Scaling the microrheology of living cells, *Phys. Rev. Letters* **87** (2001), 148102.
[16] L.G. Gamero, R.L. Armentano, J.G. Barra, A. Simon and J. Levenson, Identification of arterial wall dynamics in conscious dogs, *Exp. Physiol.* **86** (2001), 519–528.
[17] B.S. Gow and M.G. Taylor, Measurement of viscoelastic properties of arteries in the living dog, *Circ. Res.* **23** (1968), 111–122.
[18] V. Hardung, Comparative studies on the dynamic elasticity and viscosity of blood vessels, rubber and synthetic elastomers, *II Helv. Physiol. Pharmacol. Acta* **11** (1953), 194–211.
[19] J.A. Inaudi and J.M. Kelly, Linear hysteretic damping and the Hilbert transform, *J. Eng. Mech.* **121** (1995), 626–632.
[20] I.L. Jagër, Viscoelastic behavior of organic materials: consequences of a logarithmic dependence of force on strain rate, *J. Biomech.* **38** (2005), 1451–1458.
[21] M.Z. Kiss, T. Varghese and T.J. Hall, Viscoelastic characterization of *in vitro* canine tissue, *Phys. Med. Biol.* **49** (2004), 4207–4218.
[22] R.C. Koeller, Application of fractional calculus to the theory of viscoelasticity, *J. Appl. Mech.* **51** (1984), 299–307.
[23] R.L. Magin, Fractional calculus in bioengineering, parts 1, 2 and 3. *Crit. Rev. Biomed. Eng.* **32** (2004), 1–377.
[24] W.R. Milnor, *Hemodynamics*, 2nd edn, Williams & Wilkins, Baltimore, MD, 1984, pp. 78–80.
[25] M. Pagani, I. Mirsky, H. Baig, W.T. Manders, P. Kerkhof and S.F. Vatner, Effects of age on aortic pressure-diameter and elastic stiffness-stress relationships in unanesthetized sheep, *Circ. Res.* **44** (1979), 420–429.
[26] D.J. Patel, F.M. De Freitas, J.R. Greenfield and D.L. Fry, Relation of radius to pressure along the aorta in living dogs, *J. Appl. Physiol.* **18** (1963), 1111–1117.
[27] L.H. Peterson, R.E. Jensen and J. Parnell, Mechanical properties of arteries *in vivo*, *Circ. Res.* **8** (1960), 622–639.
[28] Y.A. Rossikhin and M.V. Shitikova, Analysis of the viscoelastic rod dynamics via models involving fractional derivatives or operators of two different orders, *Shock Vib. Dig.* **36** (2004), 3–26.
[29] H. Schiessel and A. Blumen, Mesoscopic of the sol-gel transition: ladder models and fractal networks, *Macromolecules* **28** (1995), 4013–4019.
[30] B. Suki, A.L. Varabais and K.R. Lutchen, Lung tissue viscoelasticity: a mathematical framework and its molecular basis, *J. Appl. Physiol.* **76** (1994), 2749–2759.
[31] S.M. Wells, B.L. Langille and S.L. Adamson, In vivo and *in vitro* mechanical properties of the sheep thoracic aorta in the perinatal period and adulthood, *Am. J. Physiol.* **274** (1998), 1749–1760.
[32] N. Westerhof and A. Noordergraaf, Arterial viscoelasticity: a generalized model. Effect on input impedance and wave travel in the systematic tree, *J. Biomech.* **3** (1970), 357–379.